Some details of the GRB experiment

INTRODUCTION

For many applications, the GRB data can be used "as is", with no corrections. However, in other cases, the user may need to be aware of several instrumental details. These are (in no particular order) spikes, dropouts, counter rollover, data compression, deadtime, pulse pile-up, and thermal feedthrough. Their relative importance depends on the type of data being analyzed. Some of these effects can be ignored, others can be corrected for, and for still others, no simple correction is possible, although simulations can be carried out to understand them (e.g. Appendix B). Note that the GRB experiment has two independent electronic circuits. One is for the real-time (i.e. untriggered) data and is based on discriminators; the other is for the triggered data and is based on a microprocessor. The two circuits have very different characteristics.

SPIKES

"Spikes" are non-statistical increases in the real-time or triggered count rate which occur in a single time bin and are considerably above the average count rate. They are generally not caused by any cosmic phenomenon, but rather, by the inability of the processing electronics and/or software to recognize changes in the operating mode quickly. Although they can have numerous causes, the most frequent one is a telemetry/ data gap. These are fairly easy to identify. An example of a spike following a telemetry gap is shown in figure 1. They can be replaced by zeros (to be ignored) or by the average count rate if a continuous data stream needs to be generated. These spikes are not real counts in the detector, but there are also spikes which are believed to be caused by particle interactions. They can trigger the burst mode of the detector, and in the high time resolution data, they are seen as events lasting 32 or 64 milliseconds. An example is shown in figure 2. It can be difficult to distinguish these events from triggers which are simply due to statistics, i.e. Poisson fluctuations. Generally, although these events are obvious in the triggered data, they tend to be diluted in the coarser resolution real-time data, and may not be evident there.

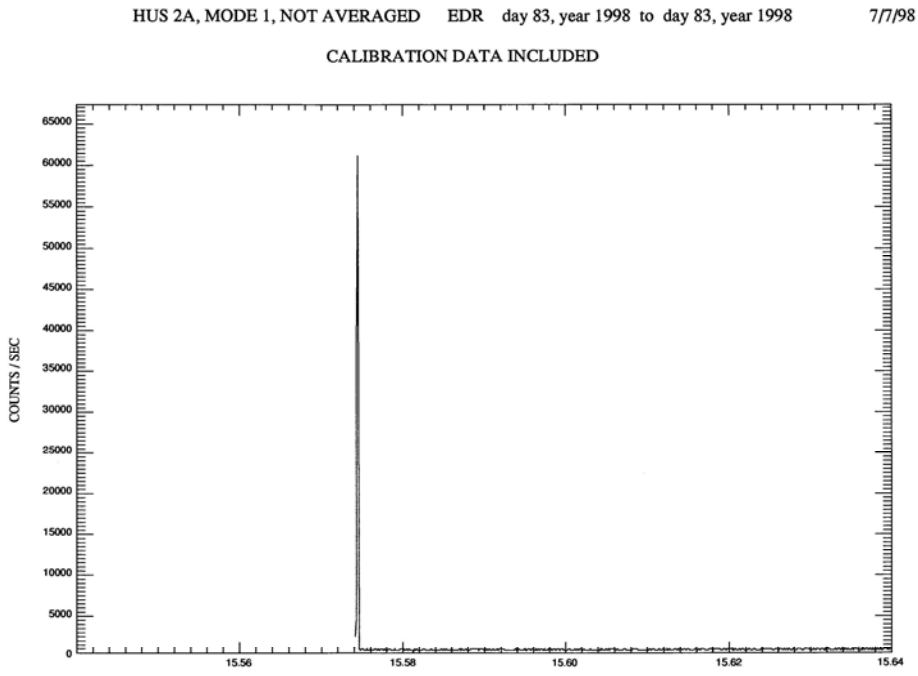

Figure 1. A spike in the real-time data following a data gap.

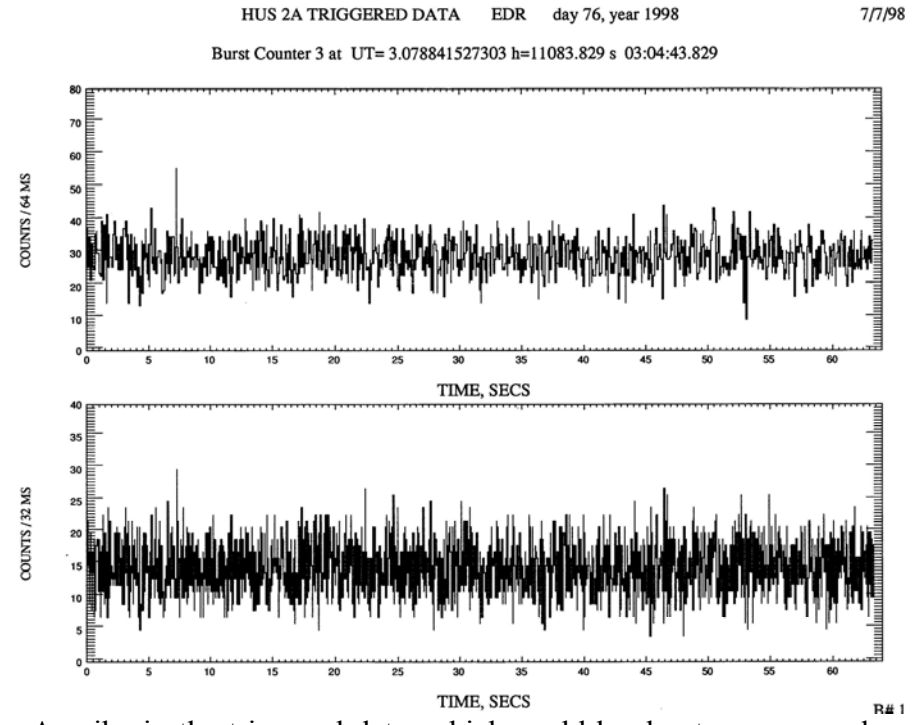

Figure 2. A spike in the triggered data, which could be due to a energy deposit from a particle, or to Poisson noise. This spike is not evident in the real-time, low resolution data.

DROPOUTS

"Dropouts" are sudden, non-statistical decreases in the apparent real-time count rate, which last for one sampling interval. They are caused by an anomaly in the processing electronics, and are fairly frequent in the data. An example is shown in figure 3. Dropouts cannot be corrected for, but they can likewise be replaced by zeros or by the average count rate.

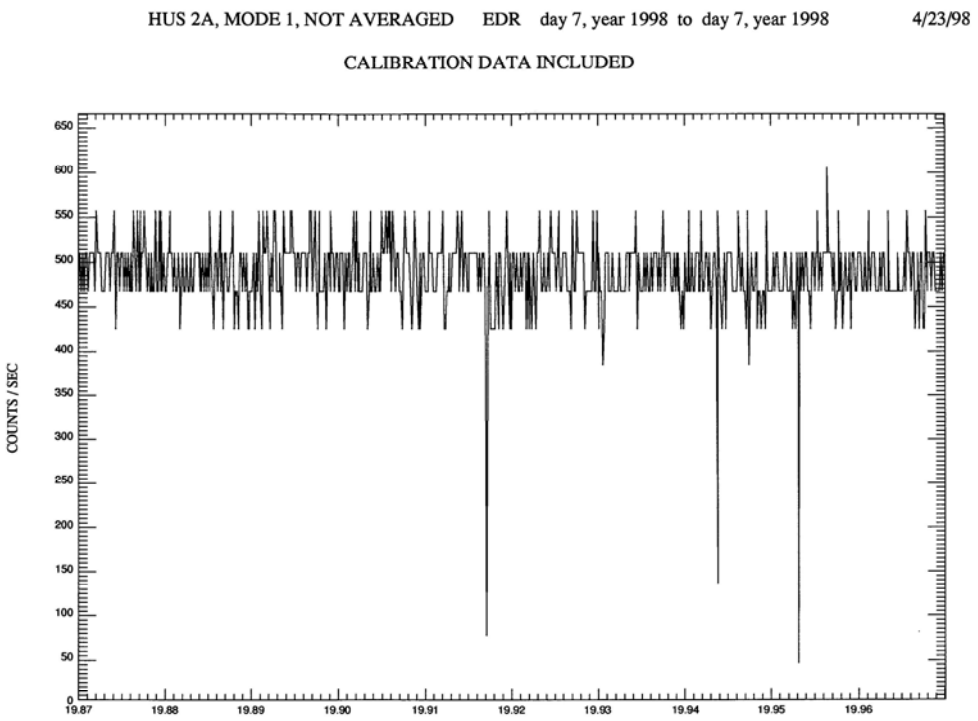

Figure 3. Data dropouts in the real-time data.

COUNTER ROLLOVER

The counters that hold the real time count rates are dimensioned to 32640. When the number of counts in a time interval exceeds this, the counter rolls back to zero and begins counting again. The observed count rate can display one of several behaviors, as shown in figure 4. In this figure, the time history of an intense solar flare on November 4 2003 is displayed. The count rates rise slowly, and a sawtooth pattern is observed at around 125 s and 160 s from the start in the black curve. This is where the counter has reset to zero and begun counting again. When the input count rate hovers at around 32640 c/s (at about 500 s from the start), then small fluctuations in the input rate can cause the counter to reset many times as the rate exceeds the maximum. In the example in figure 4, the true

rate (in red) can be reconstructed by assuming that the rates of increase and decrease in the input are relatively slow, and that the counter has only reset once when the observed rate changes. However, in some cases (for example, the rising edges of SGR giant flares) the increase in the input rate is so rapid that the counter may reset more than once between two consecutive time bins. When attempting to reconstruct the true rates in this, or any other case, it may be useful to reconstruct the falling edge of the observed time history first (because it may be decreasing at a slower rate), and to count the number of rollovers. This number must be the same as the number of rollovers in the leading edge.

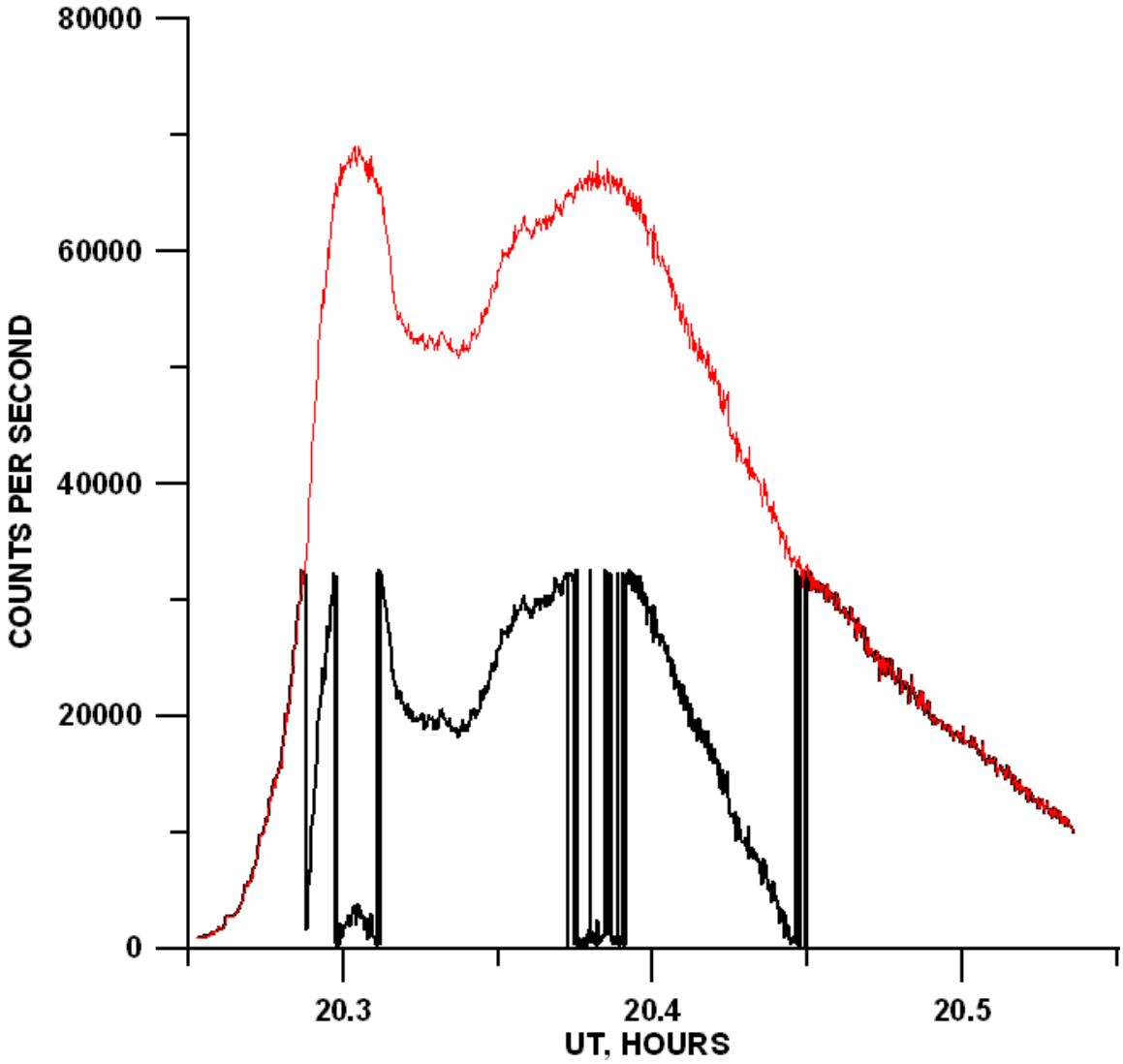

Figure 4. The observed (black) and corrected (red) time histories of the November 4 2003 solar flare, illustrating counter rollover. Note that no correction has been applied for the dead time in either curve.

DATA COMPRESSION

The real-time count rates are compressed for storage in the experiment memory according to the algorithm Cout*(Cout+1)/2=Cin. Here Cout refers to the output counts

(stored in the memory), and Cin refers to the input counts. When the count rate is low, say around the background level, the effects of compression are easily visible (e.g. figure 3), because the decompressed rates look "quantized". This effect becomes negligible at higher count rates. For most purposes, the user will only encounter decompressed rates in the archived data.

DEADTIME

Deadtime is an effect which is due to the inability of the electronics to process incoming counts rapidly enough to keep up. For the real-time data, the maximum observed count rate is around 80,000 c/s, and the response time for processing a single photon is $\tau=4.6 \times 10^{-6}$ s. Thus the observed counting rate n is related to the true counting rate N by $n=N*\exp(-N\tau)$. For most cosmic or solar events, the effects of dead time are small. However, for large events, the correction is an important one, as figure 5 illustrates.

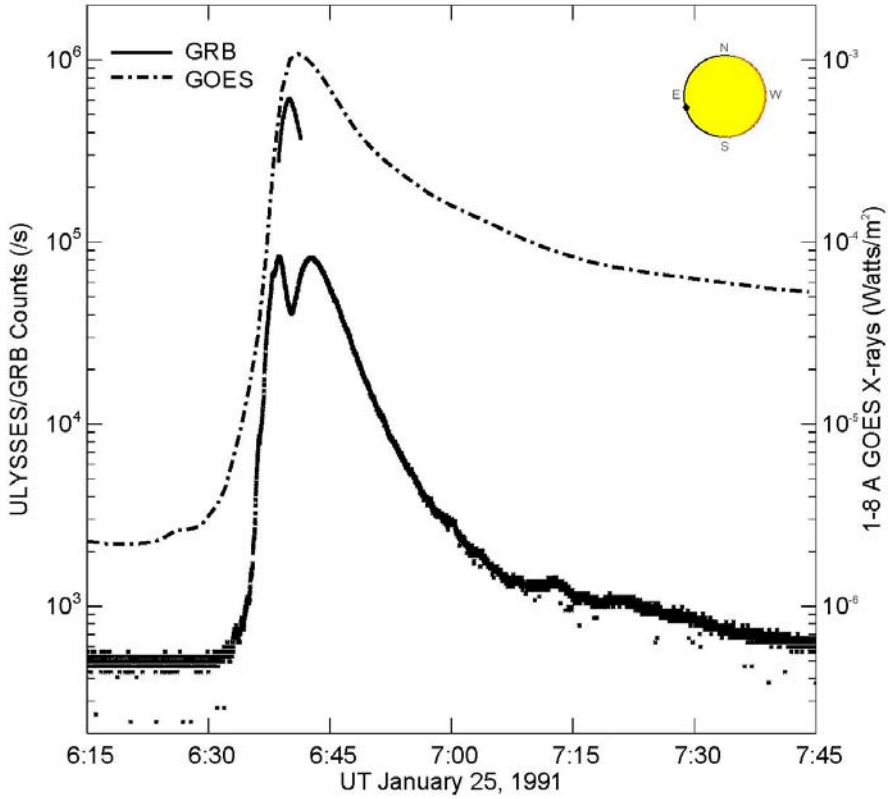

Figure 5. From "The Ulysses Catalog of Solar Hard X-Ray Flares", C. Tranquille, K. Hurley, and H. S. Hudson, 2008, Solar Physics, in press. The black dots are the observed count rates for a solar flare. The solid black curve indicates the true rates after dead time correction. Note that the system is paralyzable, which means that during the response time τ to a single count, the recovery of the circuit is extended for an additional time τ if another event is received (see, e.g. Evans, The Atomic Nucleus, p. 785 for a discussion). Thus once the true count rate increases beyond a maximum number of counts/second, the observed rate decreases.

The effects of dead time in the triggered data (both time histories and energy spectra) are considerably more complex. Jim McTiernan has studied this problem, and his analysis is given in Appendix A.

PULSE PILEUP

The following discussion of pulse pileup is taken from Tranquille, Hurley, and Hudson, The Ulysses Catalog of Solar Hard X-Ray Flares, 2008, Solar Physics (in press).

Pulse pile-up is an effect that occurs at high count rates. Two or more pulses interact in the detector within a time that is too short for the electronics to distinguish them. (See Datlowe, D.W.,1975, Pulse pile-up in hard X-ray detector systems. Space Science Instrumentation 1, 389 – 406; erratum 2, 523. and Kane, and S.R., Hudson, H.S., 1970, Re-Interpretation of OSO-III Scintillation Counter Measurements of Hard Solar X-Ray Spectra. 14, 414 – 418). The resulting signal is a single pulse whose equivalent energy is roughly the sum of the energies of the input pulses. Even if the energies of the input pulses are below the electronics threshold for detection (see Figure 6), the resulting sum signal may be above it.

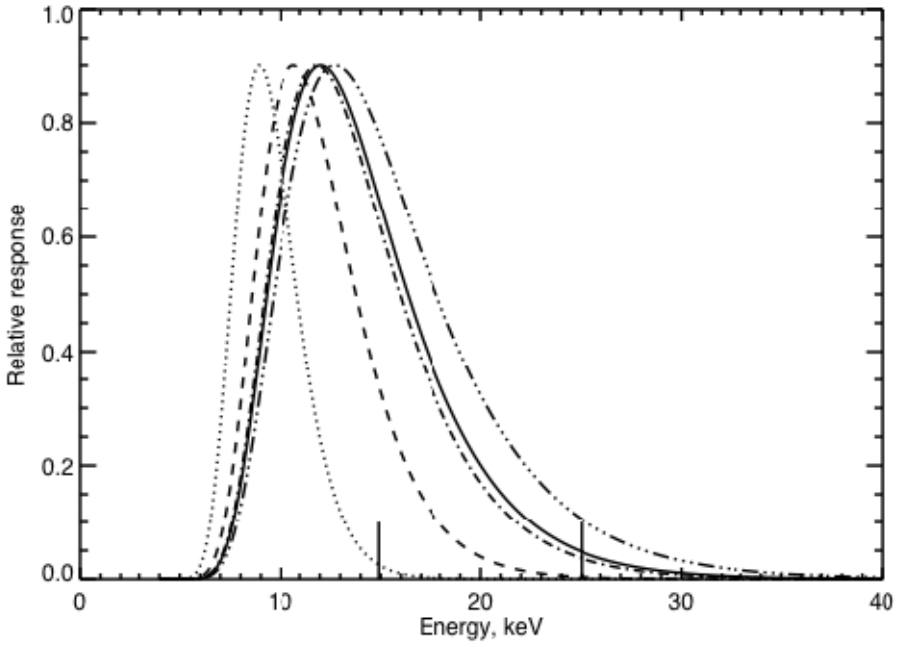

Figure 6. Model pulse height distributions for the Ulysses/GRB detector for exponential input spectra with kT = 1, 2, 3, 3.2 , and 4 keV. The solid line (kT = 3.2) shows the spectrum chosen for the pile-up studies (see Appendix B of "The Ulysses Catalog of Solar Hard X-Ray Flares", C. Tranquille, K. Hurley, and H. S. Hudson, 2008, Solar Physics, in press). The short vertical lines show (left) the minimum 50% transmission energy for GRB, and (right) the electronic channel threshold of 25 keV.

This effect can be an important one when the input spectrum is from a solar flare because of the large fluxes of low-energy photons in the thermal component of the spectrum. These pulses are below the 25 keV counting threshold and so are not counted directly, but if multiple events occur within the detection time window, their sum pulse can exceed the detection threshold and be counted. The situation is further complicated by several factors. First, without knowledge of the shape and intensity of the thermal solar X-ray spectrum, a correction cannot be calculated. Second, because the thermal counts are not directly detected, the shape of the input photon spectrum cannot be inferred from the observed pulse-height spectrum. Note that pulse pile-up is distinct from dead time effects, since the pulses that pile up do so within a dead time interval. Both effects can be present at high enough count rates.

Pile-up can be studied by Monte-Carlo simulations (see Appendix B). A very thorough Monte-Carlo program was written for the Ulysses detector, and was used to infer the influence of pulse pile-up on the spectra of major flares (Kane, S.R., Hurley, K., McTiernan, J.M., Sommer, M., Boer, M., Niel, M., 1995, Energy Release and Dissipation during Giant Solar Flares. 446, L47). We have now used this program to estimate the effects of pile-up using RHESSI observations for the input spectrum, specifically those described by Holman et al. (2003, Electron Bremsstrahlung Hard X-Ray Spectra, Electron Distributions, and Energetics in the 2002 July 23 Solar Flare. 595, L97 – L101). The thermal component of this flare had an effective temperature of 3.2 keV at maximum. We have simulated the effect that such a spectrum would have on the GRB detector for input counting rates over a wide range, as described below. The effects which we describe below are a strong function of the assumed bremsstrahlung temperature.

The Monte-Carlo program simulates the effects of a parallel beam of X-rays incident on the GRB detector on-axis (as a solar flux would approximately be). Compton and photoelectric K- and L-shell interactions in the hemispherical geometry of the CsI crystals are taken into account, as are Auger electrons, fluorescence, photon scattering out of the crystal, and the escape of scattered electrons. The crystal resolution as a function of energy, and the 0.03 cm thick Al window are also taken into account. For the simulations described here, a bremsstrahlung-like exponential spectrum was used as input between 1 and 150 keV. We refer to the input as photons, to distinguish it from the detected counts. The input count rate was varied between 10^3 and 10^7 photons s^{-1} with a Poisson interval distribution, and the detected count rate due to piled-up photons was recorded in the 25-150 keV energy range. If two or three photons interacted in the detector within a time interval less than one microsecond (the approximate shaping time constant for the GRB detector), they were counted as a single, piled-up count whose energy was the sum of the energies of the original photons. More than three pile-ups were not tracked, but they will contribute too at very high input count rates. Each simulation used 10^6 input photons.

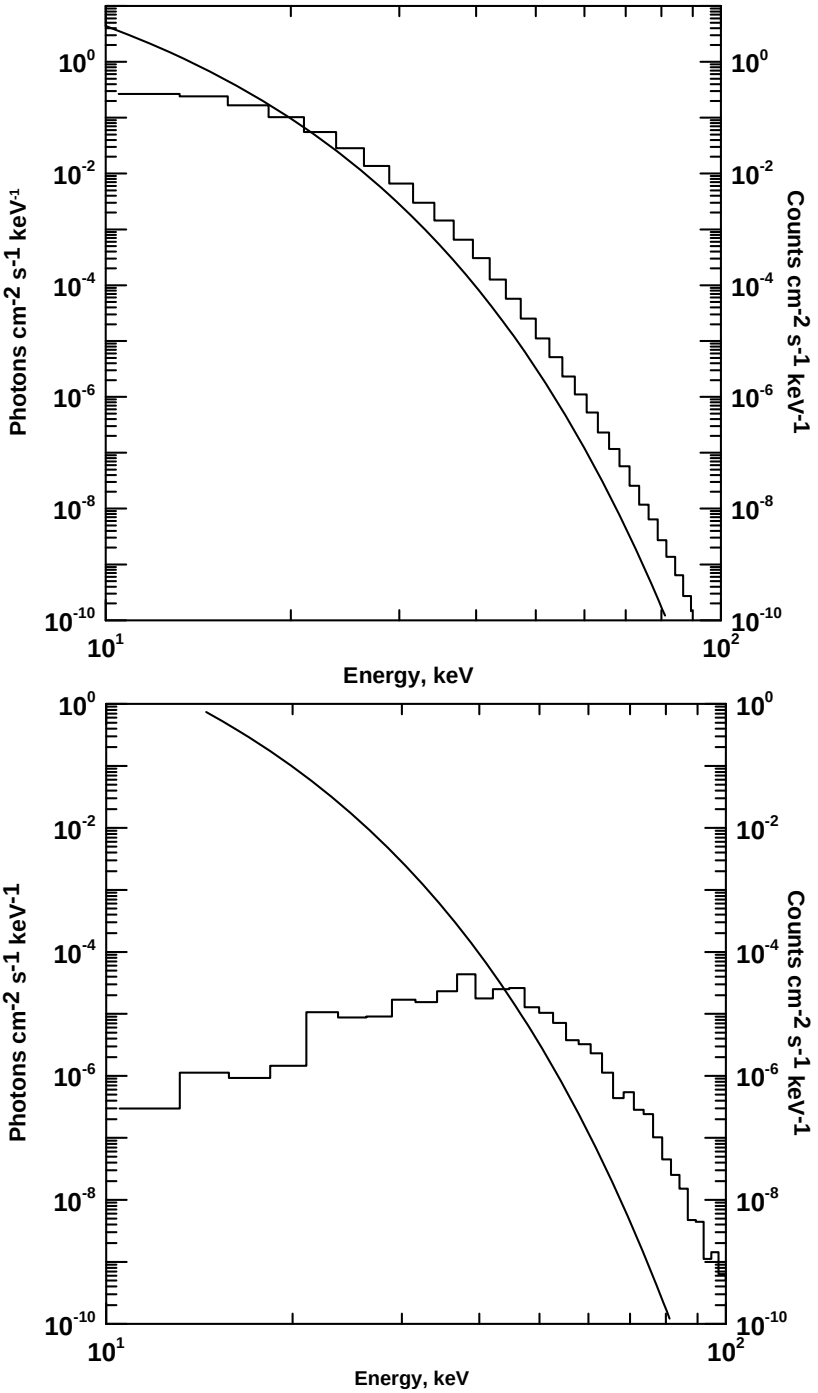

Figure 7. Smooth curve: a 3.2 keV bremsstrahlung spectrum. Histogram: the resulting spectrum in the GRB detector, calculated by the Monte-Carlo program. Input rates of 10^3 photons s^{-1} (top) and 10^7 photons s^{-1} (bottom) were assumed. For the input rate of 10^3 photons s^{-1}, the output spectrum follows the input spectrum above about 20 keV, and is attenuated below it due to the entrance window. Pile-up is negligible. For the higher input count rate, the output spectrum is severely attenuated below about 35 keV due to pile-up, and many of these piled-up photons appear between 35 and 200 keV.

Figure 7 shows the input photon and output count spectra for 10^3 and 10^7 photons s^{-1}. At 10^3 photons s^{-1}, the output count spectrum follows the input photon spectrum above an energy of about 20 keV. Below this energy, the input photon spectrum is strongly attenuated due to the Al entrance window (for a parallel input beam, its effective thickness is 0.03 cm only for a single, on-axis point, and increases off-axis due to the hemispherical geometry). At 10^7 photons s^{-1}, the output count spectrum is attenuated severely below about 35 keV, due to photon interactions which pile up and are counted at higher energies. The count spectrum above 35 keV clearly reflects this phenomenon. Figure 8 summarizes some of these results. The bottom X-axis shows the input photon rate at the GRB detector over the 1-150 keV range for a bremsstrahlung-type exponential spectrum with kT = 3.2 keV. This is converted into W m^{-2} at 1 AU in the GOES soft channel along (the upper X-axis), so that the count rates can be compared to GOES fluxes, using the scaling law derived in Section 4.2 of Tranquille et al. (2008). The Y-axis shows the piled-up count rate for the GRB experiment in the 25-150 keV range. The piled-up count rate is calculated for assumed GRB solar distances of 1 AU and 3.2 AU from the Sun in Figure 8. The figures show that pile-up is negligible for input photon rates up to about 10^5 photons s^{-1}. Even at 10^6 photons s^{-1}, where the average interval between counts is only 1 μs, that is, one pulse-shaping time, the piled-up count rate is small compared to the input photon rate. This can be understood as the result of several factors. First, the input photon rate is measured over a wider energy range, 1-150 keV, than the piled-up count rate (25-150 keV, the GRB passband). Second, for photons to actually pile up into the GRB passband, they must traverse the entrance window and deposit energies whose sum falls between 25 and 150 keV; many interactions, although piled-up, result in smaller energy deposits, and would not be counted. Finally, the input photon fluxes are quite small at energies above 20 keV compared to the 1 keV fluxes, due to the shape of the bremsstrahlung spectrum; thus, while they can pile up and fall into the passband, their numbers are very small. We emphasize that two effects have not been treated here. The first is the pile-up of more than three simultaneous pulses. This will dominate over double and triple pile-ups at input photon rates above $\sim 3\times10^6$ counts s^{-1}, and therefore the piled-up count rates in Figure 8 at these input photon rates should be considered very conservative lower limits. (Note that this does not imply that multiple pile-ups are an important factor in contaminating the observed spectra, simply that they are more frequent than double and triple pile-ups. The rates of the latter are very small compared to the input photon spectrum, and the rates of multiple pile-ups are expected to be small, too.) The second is the pile-up of thermal input photons with non-thermal ones; we have not assumed any non-thermal component in these simulations.

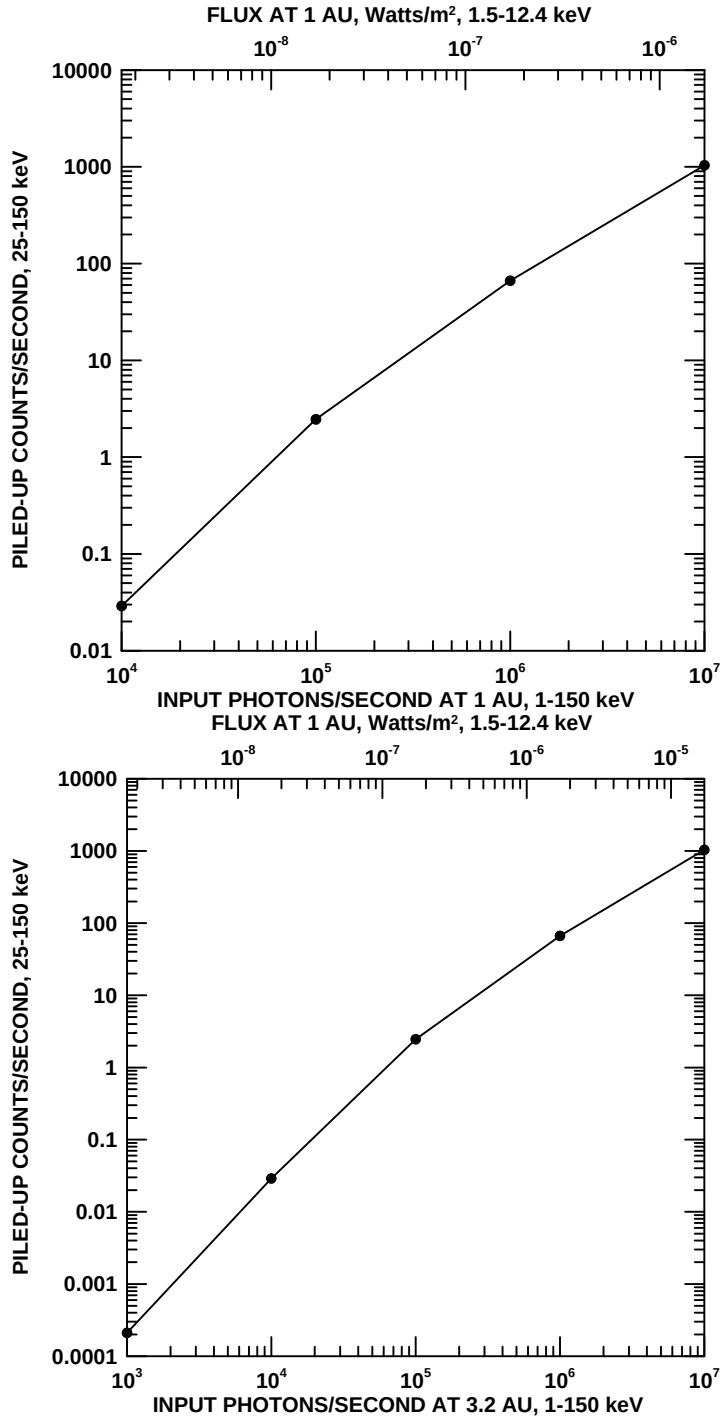

Figure 8. Summary of the Monte-Carlo results for Ulysses at 1 AU (top) and 3.2 AU (bottom) from the Sun. A 3.2 keV thermal bremsstrahlung spectrum was assumed, and one million photons were tracked. The lower x-axis gives the input count rate over the GRB detector between 1 and 150 keV. The y-axis shows the rate of double and triple pile-ups in the 25-150 keV GRB energy band. Note that it is a small fraction of the input rate. The top x-axis gives the equivalent flux for a 3.2 keV bremsstrahlung spectrum in the 1.5-12.4 keV band, for comparison with GOES rates.

THERMAL FEEDTHROUGH

Thermal feedthrough is an effect whereby a low energy thermal spectrum (such as that from a solar flare) contributes to the high energy count rate of a detector with broad energy resolution. An incoming photon with energy E has a probability of being recorded with energy E' in a scintillation detector like the GRB, where E' follows a Gaussian distribution. Thus incoming low energy photons, below the detector's electronic threshold, are actually recorded as counts above the threshold. The problem can become a severe one for intense solar flares. The following discussion of thermal feedthrough is taken from Tranquille, Hurley, and Hudson, The Ulysses Catalog of Solar Hard X-Ray Flares, 2008, Solar Physics (in press). Note that thermal feedthrough effects can be calculated with the Ulysses Monte Carlo program (Appendix B).

To study effects such as thermal feedthough, we have done a Ulysses–RHESSI comparison for the GOES X8.3 solar flare of November 2, 2003. Broad-band hard X-ray photometry of solar flares poses particular problems in reconciling the intense thermal component, usually characterized by a maximum kT in the range 1-2 keV, and the much fainter non-thermal tail produced mainly by 10-100 keV electrons. RHESSI partially solves this problem by having a set of shutters that control the absorber thickness across the detector. All other solar hard X-ray spectrometers have fixed windows (that of Ulysses is 0.3 mm Al in a hemispherical dome configuration). The entrance window serves as a high-pass filter which determines the distribution of pulse heights; in the case of GRB the half-transmission energy thus works out to be about 15 keV, but the steepness of the thermal source spectrum pushes the peak in the pulse-height spectrum to below 10 keV for the lower temperatures. These counts can still contribute to the 25-150 keV observational window, however, via resolution broadening and via pulse pile-up (discussed above).

Figure 6 shows the essential elements for a model representation of the pulse-height spectrum produced by a solar thermal source. Note that the peak of the pulse-height distributions fall well below the electronics threshold, and even below the 50% transmission energy of the entrance window. The high-energy tail of these pulse distributions competes with the true hard X-ray spectrum. This causes the morphologically smoother light curves seen at lower hard X-ray energies, seen not just with Ulysses/GRB but with most other scintillator-based spectrometers.

The comparison of counting rates with RHESSI provides essentially complete diagnostics, since RHESSI has high spectral resolution and is not limited to a single telemetry band (25-150 keV) as GRB is. We show the direct comparison in Figure 9, which illustrates a satisfactory comparison early in the event, then a growing divergence later on. The RHESSI live time reached a minimum of about 15% near the time of peak counting rates, and at 25 keV also exhibited the smooth late excess – though not so large – as found in the GRB counts. This behavior can be explained by the poorer spectral resolution of GRB, which is determined by its on-board calibration to be about 48% at 25 keV. There is no need to invoke pulse pile-up for this event, and the dead time corrections for both instruments also seem satisfactory.

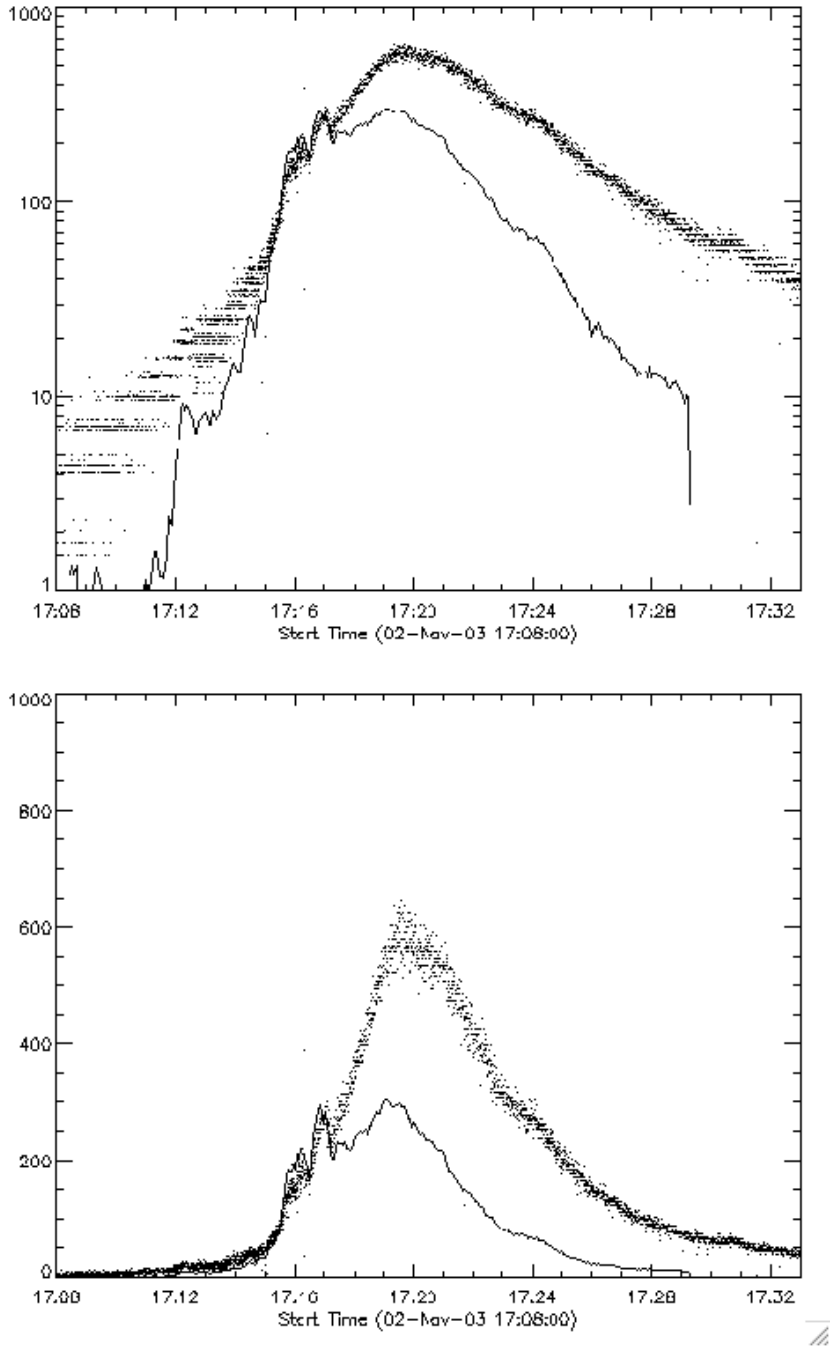

Figure 9. Comparison of RHESSI counting rate (line) with GRB counting rate (dots) for 25-150 keV during the X8.3 flare of November 2, 2003. Top, log display; bottom, linear. We attribute the discrepancy after about 17:17 UT to the increasing emission measure of the thermal component directly detected by GRB, rather than via pile-up. During the impulsive phase there is good agreement.

Appendix A. Dead Time in the GRB Triggered Data

In-flight Calibration of the Ulysses Dead-time Correction

J. M. McTiernan

Space Sciences Laboratory, Univ. of California Berkeley

18-Feb-1997

1 The Dead-time Correction for Ulysses Spectral Data

The system used to obtain energy spectra for the Ulysses GRB detector works like this: A photon is processed by an ADC, then transmitted to the microprocessor, and acquired by the microprocessor. The time for the first step varies with photon energy, the time for the second step should be constant, and the third step is variable. The time to process a photon in the ith channel was measured to be

$$\tau_i = [1 + 0.47(4i - 1.5)/25000.0] \ . \tag{1}$$

This is expected to be a nonparalyzable system, which means that any photon that arrives during the time when another photon is being processed is ignored. If channel i counts n_i counts/sec, and if no other channel is counting, then the circuits are dead for the fraction of time given by $n_i\tau_i$. When more than one channel is counting, the fraction of time that the circuits are dead is given by $\sum n_i\tau_i$, and the fraction of time that they are live is $1 - \sum n_i\tau_i$. This is the probability that a photon in any channel can be recorded, so that if the jth channel records a count rate of n_j, the true incident count rate is given by

$$N_j = n_j/(1 - \sum n_i\tau_i) \tag{2}$$

The resulting dead-time correction factor,

$$\tau_d = 1/(1 - \sum n_i\tau_i) \tag{3}$$

is the same for each channel.

1.1 Comparison of Spectral Data and Integral Count Rate

In addition to the spectral data, the Ulysses detector measures the count rate between two energy levels, typically between 20 and 150 keV. This energy range is similar to that covered by the highest 14 channels of the spectral data (e.g., for the flare of 15-nov-1991 22:37 UT, the rate data covers the range of 19.9 to 165.5 keV, and the top 14 channels of the spectral data range from 20.7 to 165.5 keV). Thus, after correcting for dead-time, the total count rate in the 14 highest channels should be close to the integral count rate. Since the energy levels are not identical, the rates will not be exactly the same, but the difference can be calculated given an idea of the photon spectrum. For the levels given above, and typical flare spectra with spectral indices m = 2.5 to 7, the difference ranges from approximately 5% to 20%.

For real data this is true for low count rates, but as the count rate increases, the agreement between the integral rate and the total of the spectral data falls apart. This is shown here in fig 1, which compares the integral rate data with the total of the highest 14 channels of the spectral data (the line with + signs). The agreement is good early in the flare, but at the flare peak, the spectral count rate is much higher, reaching a peak rate of 4100 cps, as opposed to the peak rate of 3360 cps. This is an overestimate of 21%.

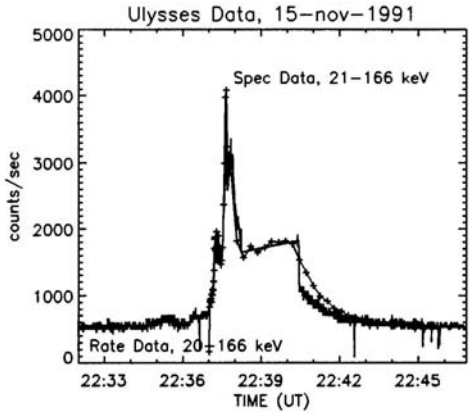

Figure 1: Time profiles for the Ulysses integral count rate data and the total of the upper 14 channels of the spectral data, for the flare of 15-nov-1991. The spectral data is denoted by the line with plus signs.

The discrepancy also shows up in fitted spectra; fig 2 shows the Ulysses spectrum for the peak 8 second interval of the same flare, plotted with the Yohkoh HXS spectrum. The Ulysses flux is always higher, with the difference increasing with energy. The Ulysses flux at 25 keV is 34% higher than the HXS flux, and the Ulysses flux at 160 keV is a factor of 3 times the HXS flux.

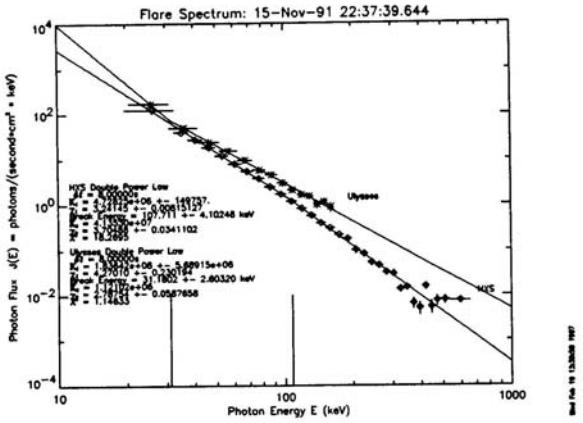

Figure 2: Spectra for the flare of 15-nov-1991, at the flare peak, from 22:37:39 to 22:37:47 UT. The Ulysses spectrum is denoted by stars and the Yohkoh HXS spectrum by diamonds.

We know that for high count rates, the spectral dead-time correction factor, as shown in eqn 2 becomes infinite, and then negative; for a large enough observed count rate, typically a total of 3000 cps, the sum $\sum n_i \tau_i$ approaches unity, and there is zero live time. But as shown in fig 1, things fall apart much earlier; the peak observed spectral count rate for the 15-nov-1991 flare is only 1600 cps.

1.2 Using the Rate Data to Obtain a New Dead-time Correction

So we suspect that the dead-time correction is not quite correct. We can try to get a better value for the spectral dead-time factor using the integral rate data. The procedure is as follows: First, find the spectral index before applying any dead-time correction. From this we can find an expected value for the integral count rate, by integrating the non-dead-time corrected spectrum over the detector response. The new dead-time correction is then the observed rate data divided by the expected rate data. Plots of the observed rate, and the rate expected from the non-dead-time

corrected spectra for the 15-nov-1991 flare are shown in fig 3.

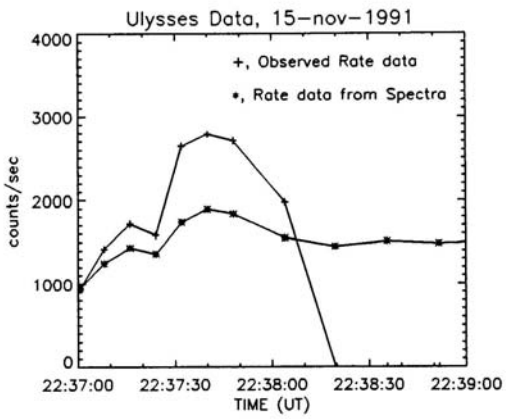

Figure 3: The observed integral rate data for the 15-nov-1991 flare (plus signs), and the expected rate calculated from the non-dead-time corrected spectral data (stars).

The next plots, fig 4, show a comparison of the new dead-time correction with the old one. The top panel shows the two corrections, and the bottom show the ratio of the old and new dead-time correction factors. Note that the new correction factor is always less than the old factor, and that the difference increases with increasing count rate. This is the behavior that we hope for.

1.3 Spectral Comparison

Given the new dead-time factor, we can go back and look at the spectrum; this is shown in fig 5, compared again with the Yohkoh HXS spectrum. The agreement is much better, at all energies.

Note that the new Ulysses spectrum is not only lower at each energy, but it is also steeper than the original spectrum. The original spectrum had a spectral index of $m = 2.8$, while the new spectrum has a spectral index of $m = 3.0$. (For HXS, the index over the same energy range is 3.2.) This is true even though the dead-time correction is the same for all channels. This happens because the dead-time correction is applied to the total count rate in each channel and the spectrum is calculated from the background-subtracted excess count rate. The effect on the excess count rate is larger for higher energies, because the signal-to-noise ratio is much smaller. For example, in the 20-30 keV Ulysses channel, the count rate is 1860.11 cps with the old dead-time correction. With

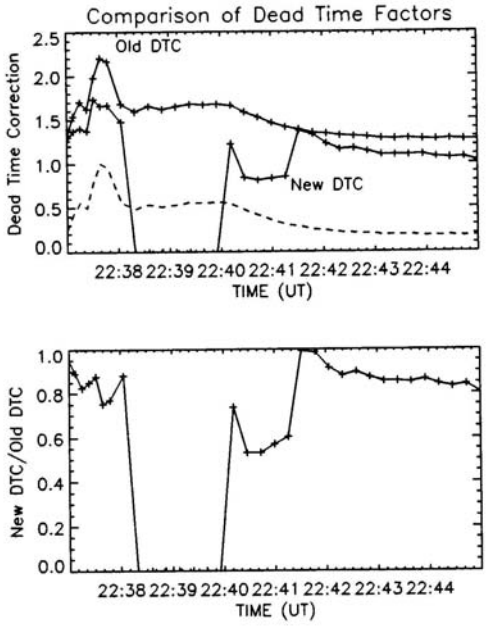

Figure 4: Top panel: the old and new dead-time corrections for the 15-nov-1991 flare, the dashed line is the time profile of the observed spectral count rate. The gap from 22:38:20 to 22:39:55 is there because the rate data was zero for that period. Bottom panel: the ratio of the corrections.

the new correction, the rate becomes 1456.11, a reduction of 22%. The old and new background rates are 154.63, and 145.70, respectively, so that the old and new excess count rates are 1705.48 and 1310.41, a difference of 23%. In the highest channel, 145-155 keV, the original and new total count rates are 14.04 and 10.99, the original and new background rates are 8.64 and 8.14, and the original and new excess count rates are 5.40 and 2.85. The reduction in the excess rate here is 47%. For low energies, the signal-to-noise is large, so that the difference in excess rate is similar to the difference in the total rate. For high energies, the signal-to-noise is small, and a small difference in total count rate results in a large difference in excess count rate.

Fig 6 shows comparisons of the total and excess count rates for the old and new dead-time corrections for the 15-nov-1991 flare. The top plot shows the total count rates; the solid line is for the old dead-time correction and the dashed line is for the new correction. The bottom plot shows

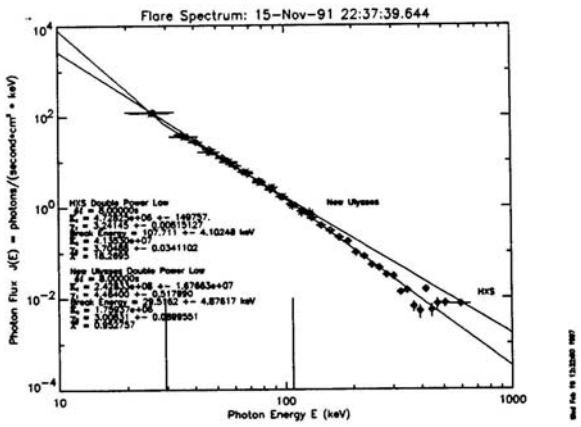

Figure 5: Spectra for the flare of 15-nov-1991, at the flare peak, from 22:37:39 to 22:37:47 UT' The Corrected Ulysses spectrum is denoted by stars and the Yohkoh HXS spectrum by diamonds.

the same comparison for the excess count rate. It is clear that the difference increases with energy.

The ratio of the old count rates to the new count rates is shown in fig 7. The solid line is the ratio of the total count rates, and is, of course, a constant. The dashed line is the ratio of the excess count rates, showing clearly that the effect is larger for higher energies. This is why the spectrum is steeper.

1.4 Fits to the New Dead-time Correction

As seen above in figure 4, we can only use this method for time intervals where there is rate data. Also we need to calculate the spectrum for each interval before using the new correction. Life would be easier if we had some way to apply the new correction for intervals for which there is no rate data, and also one for which we do not need to know the spectrum.

We can attempt to do this by calculating the new correction for every available spectrum, and the trying to fit it. Fig 8 is a plot of the new dead-time correction versus total observed count rate for 1791 different intervals for 131 flares. The line is a fit to the data, given by the expression

$$\tau_d = 1.0 + 0.659247C + e^{4.51938(C-3.32271)} + 0.674580 * e^{-0.412131(C-3.01159)^2} \quad (4)$$

where τ_d is the dead-time correction factor, and C is the total count rate in the highest 14 channels,

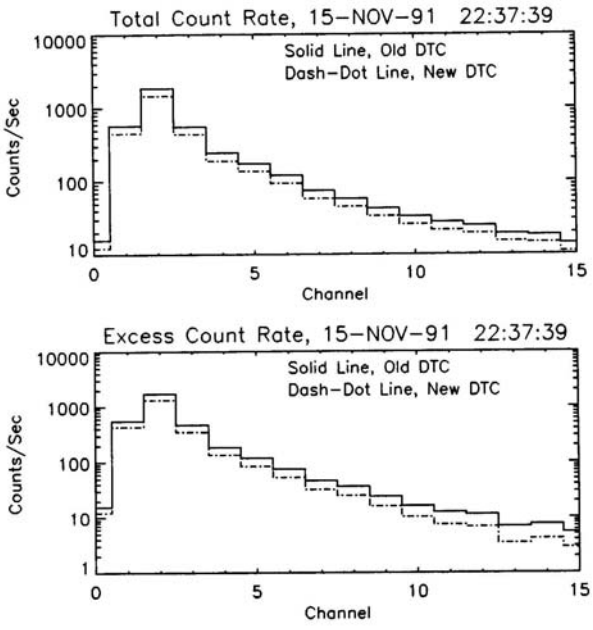

Figure 6: Top panel: total count rate versus channel number for the peak interval of the 15-nov-1991 flare. Bottom panel: Excess count rate for the same time range. The solid line is for the old dead-time correction and the dash-dot line is for the new correction.

divided by 1000. This expression fits the corrected dead-time factors well for high count rates, but tends to overestimate the correction for low count rates. Also, it is optimized for spectra with spectral indices of 3 to 5, so it is not accurate for very soft or hard spectra. For low count rates, it seems to work better if we retain the form of eqn 2 while using a different time constant for τ_i; this results in

$$\tau_d = 1/(1 - \sum n_i \tau_i) \ , \tag{5}$$

where

$$\tau_i = [1 + 0.47(4i - 1.5)/32500.0] \ . \tag{6}$$

A plot of this version of τ_d is shown along with the original fit in fig 9. This method fits the low

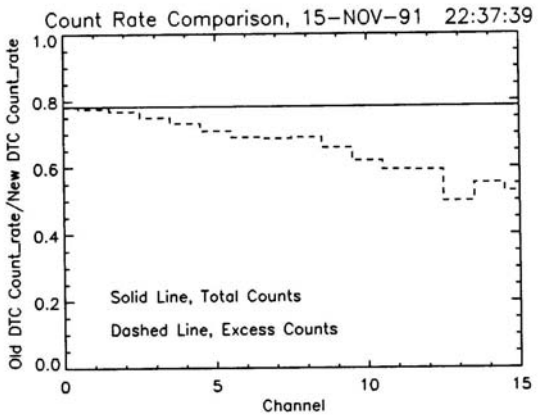

Figure 7: The ratio of the count rates for the old and new dead-time correction. The solid line shows the ratio for total counts, and the dashed line shows the ratio for excess counts.

count rate data, and depends on the photon spectrum as does the original correction factor. This correction is now the default in QUICK_USPEC, the Ulysses spectral fit program.

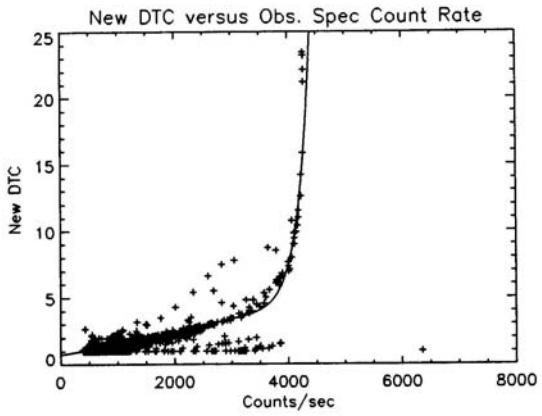

Figure 8: The new dead-time correction versus total observed count rate (in the upper 14 channels of Ulysses), for 1791 intervals of 131 flares. The line is fit to the data, of the form $1 + a_0 x + e^{a_1(x-a_2)} + a_3 e^{a_4(x-a_5)}$.

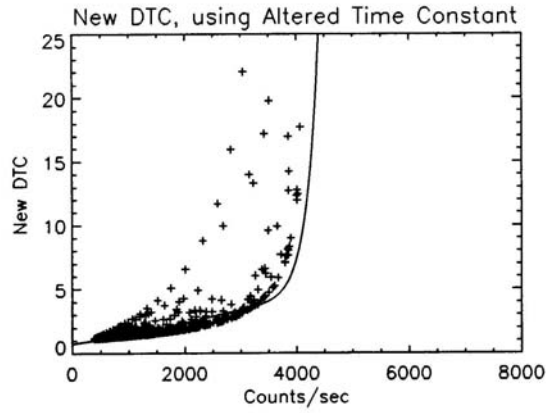

Figure 9: The dead-time correction obtained using the altered time constant, versus total observed count rate. The line is the fit to the data.

Appendix B. The Ulysses Monte-Carlo program and the detector response matrix

ULYMC is a FORTRAN program which simulates the response of the GRB detector to various types of input spectra. It is written in FORTRAN 77 on a Sun Ultra 5, but it can probably be ported fairly easily to other systems. The program takes into account, among other effects, pulse pile-up (up to three photons), thermal feedthrough, the hemispherical detector geometry, including the Al entrance window, and resolution as a function of energy. It was written to provide a description of the way the GRB detector responds to solar and cosmic events.

The input is taken from FILE.mci (input unit 1, see example below), which specifies the type of input photon spectrum (line 1) and channel numbers for integrating the output spectrum (lines 2 and 3). A comparison spectrum can be input starting a line 4, or it can be bypassed, as in the case shown. Line 5 specifies a bremsstrahlung spectrum with kT=3.2 keV, which was used to study pulse pileup. (A user-generated input spectrum may also be specified; it is read from unit 2, FILE.spc.) Line 6 gives the lower and upper energy limits for the detector, in MeV, and should not be modified. Line 7 gives the total number of photons to be treated. Line 8 gives the detector inner and outer radii, and the thickness of the dead layer. This line should not be modified. Line 9 gives the threshold energy and the number of MeV per channel for the detector response matrix (one of the program outputs) and should not be changed. Line 10 specifies parameters for the two GRB detectors, and should not be modified. Line 11 gives the initial direction cosines for the input photons; the program is optimized for photons in a parallel beam along the detector axis. Line 12 is the analog electronics time constant, and should not be modified. Line 13 gives the number of input photons per second.

```
FUNCTION
10 58
0  0
0  0. 0.
'BS' .0032
.001 .150
100000
2.24 2.54 0.00
0.00 0.00263
0.00 0.00973 .5 3.5 0.00 0.00907 3.5
0. 0. -1.
1.E-6
1.E7
```

ULYMC generates several output files. Unit 7 is a printer file; it is commented out, so the output is written to a file called fort.7. Unit 17 contains the output count spectrum in a format that is convenient for plotting programs. The full output is written to unit 25 (FILE.output). Finally, ULYMC writes a file in HPGL which is suitable for HP plotters, on unit 3; this is commented out, so that the output is written to fort.3, which can be converted from HPGL to other formats, if desired. (For example, this file can be converted to postscript using hp2xx, which is available at several websites.) Other output files (units 4, 5, 8, 9, and 10) may be ignored.

A sample output file (fort.7) is included. This file has been stripped of printer control characters, but otherwise represents the output which a user would obtain using the above input FILE.mci. Due to roundoff errors, some photon trajectories (identified in the two lines starting X2,AXO,…) are outside the crystal, some fluxes (123 out of 100000) are negative, and some photons (49 in this example) appear to have interacted in the dead layer. These can be ignored.

For simple applications, where it is necessary to check the consistency of an observed spectrum with a model spectrum, the XSPEC program may be used (http://heasarc.gsfc.nasa.gov/docs/xanadu/xspec/). The GRB response matrix is xspec.drm (a FITS file).